ARMA 24–0097

A graph-based drained wellbore stability analysis in Mohr-Coulomb rock formation under hydrostatic in situ stress field

Wang, X. and Chen, S.L.
Department of Civil & Environmental Engineering, Louisiana State University, Baton Rouge, LA, USA
Han, Y.H.
Aramco Research Center at Houston, Aramco Americas, Houston, TX, USA
Abousleiman, Y.
Integrated PoroMechanics Institute, School of Geosciences, Mewbourne School of Petroleum & Geological Engineering, The University of Oklahoma, Norman, OK, USA

This paper was prepared for presentation at the 58th US Rock Mechanics/Geomechanics Symposium held in Golden, Colorado, USA, 23-26 June 2024. This paper was selected for presentation at the symposium by an ARMA Technical Program Committee based on a technical and critical review of the paper by a minimum of two technical reviewers. The material, as presented, does not necessarily reflect any position of ARMA, its officers, or members. Electronic reproduction, distribution, or storage of any part of this paper for commercial purposes without the written consent of ARMA is prohibited. Permission to reproduce in print is restricted to an abstract of not more than 200 words; illustrations may not be copied. The abstract must contain conspicuous acknowledgement of where and by whom the paper was presented.

ABSTRACT: This paper focuses on the development of a rigorous analytical solution for the drained wellbore drilling problem in a non-associated Mohr-Coulomb rock formation subjected to hydrostatic in-situ stress field, for a specific case that the axial/vertical stress is strictly the intermediate principal stress in the drilling process. The proposed solution is extended from the graphical analysis-based method recently proposed by Chen in 2024 for the cylindrical cavity expansion problem. The wellbore support pressure versus the contracted borehole radius, i.e., the well-known wellbore drilling curves, are numerically calculated through the radial equilibrium equation in the Lagrangian form. The graphical solution effectively avoids the common yet unnecessary intermediacy assumption for the axial/vertical stress in most existing wellbore drilling analyses. Selective numerical results are presented for the desired wellbore drilling curves and the impacts of some rock mechanical parameters on the calculated curves are also investigated.

1. INTRODUCTION

Wellbore drilling in the petroleum industry is a process whereby natural resources, such as natural gas and oil, can be extracted from the rock formation. Wellbore stability must be maintained during both wellbore drilling and the well construction phase to support the structural integrity an oil and gas well. In the wellbore drilling, the rock mass inside the circular borehole is relaxed progressively and removed eventually, which results in the wellbore contraction. The stress field around the wellbore will also be redistributed, which is therefore necessary to be determined during the drilling process (Risnes et al., 1982).

In the past few decades, the stress field around the wellbore undergoing drilling is primarily obtained based on the linear elasticity or poroelasticity theory (Al-Ajmi & Zimmerman, 2006; Bradley, 1979; Carter & Booker, 1982; Cui et al., 1997; Detournay & Cheng, 1988; Kanfar et al.; 2015; Mehrabian & Abousleiman, 2013). However, the rock mass around the wellbore will develop plastic deformation, which is inevitable in many scenarios (Charlez, 1997; Papanastasiou & Zervos, 2004; Potts & Zdravkovic, 1999). It follows that plastic deformation of rock occurs due to high stresses concentrated near and around the wellbore during active drilling operations (Ito, et al., 1998; Zoback, et al., 2003). The stress distribution determined based on the elastic analysis will be invalid after the rock mass runs into plasticity (Chen, et al., 2011; Huang, et al. 2018). Note that the plastic yielding state of a rock mass depends upon the stress state, the strength properties of the rock mass around the wellbore, and the plastic yield criterion for the rock mass. It should be emphasized that the end of the pure elastic deformation does not indicate the failure of the rock mass around the wellbore. Furthermore, an allowable tolerance plastic yielding around the wellbore induced by the drilling will not affect the wellbore stability but can reduce the collapsed mud weight subsequently the cost of the drilling job. It is, therefore, necessary to evaluate the elastoplastic behavior of the rock mass around the wellbore under the drilling process.

The wellbore drilling process can be conceptualized as a cylindrical cavity contraction problem since the radial stress acting on the wellbore gradually decreases in the drilling operation. It is possible to solve the cavity contraction problem analytically with the use of Mohr-Coulomb plasticity model because of the simplicity of the geometry and yielding/boundary conditions involved. Many analytical elastoplastic solutions in the literature are developed for the cavity expansion problem (Carter et al., 1986; Chadwick, 1959; Mantaras & Schnaid, 2002;

Papanastasiou & Durban, 1997; Vesic, 1972; Yu & Houlsby, 1991), i.e., in the case that the wellbore pressure is higher than the initial in-situ radial stress at the wellbore. Note that these well-developed analytical solutions for the cavity expansion problem cannot be directly applied to the cavity contraction problem because the elastoplastic solution for cavity problems is stress-path dependent. Fortunately, the methods for solving the cavity expansion problem can be successfully applied to the cavity contraction problem through mathematical derivation. However, most analytical solutions for the cavity expansion problem in rock mass obeying the Mohr-Coulomb yielding criterion have a common drawback in that the vertical/axial stress is assumed to be the intermediate principal stress with respect to the radial and tangential principal stresses. The main reason for introducing such an assumption was to avoid the corner singularity of the Mohr-Coulomb failure envelope so that closed-form or semi-closed-form solutions can be obtained. To overcome such drawback, a so-called zoning method has been adopted to abandon this assumption (Florence & Schwer, 1978; Reed, 1988; Risnes et al., 1982), which essentially divides rock mass around the wellbore into various annuli through different orders of the principal stresses. However, the zoning method introduced in the above contributions did not seem able to clearly describe the variation of the stress field under the drilling process. Other limitations in the existing work include the assumptions of both small-strain deformation and associated plastic flow rule (Risnes et al., 1982; Reed, 1988).

To remove the constraints implied in the existing elastoplastic solutions, Chen (2024) recently developed a rigorous and complete solution for the drained cylindrical cavity expansion problem with the Mohr-Coulomb yield criterion and arbitrary coefficient of the earth pressure at rest. The essential feature of the method adopted by Chen (2024) is developed from a full Lagrangian framework-based graphical method in Chen and Wang (2022) for solving the undrained cavity expansion problem. The distinctive advantage of this novel graphical method is that the stress path pertinent to the cavity expansion problem becomes completely trackable through unique and rigorous geometrical analysis. The solution for the cavity expansion problem in the Mohr-Coulomb rock mass can be rigorously solved without adopting the intermediate assumption for the vertical/axial stress.

Through the application of the analytical solution in Chen (2024), a specific case for the cavity contraction problem in non-associated Mohr-Coulomb rock formation under the hydrostatic initial stress field is discussed in this work, i.e., the vertical/axial stress strictly remains as the intermediate principal stress in the wellbore drilling process. The orientation of the deviatoric stress path for a rock element in the wellbore wall can be determined from the magnitudes of (radial, tangential, and vertical) strain increments. The deviatoric stress path is comprised of two straight lines, including the horizontal deviatoric stress path representing pure elastic deformation, and the inclined stress path representing elastoplastic deformation. The large deformation is involved in the elastoplastic analysis. Parametric studies are performed to investigate the impacts of the friction angle, cohesion, and shear modulus on the variations of the normalized wellbore support pressure with borehole radial displacement under the drained condition. The critical mud pressure required to maintain the wellbore stability is discussed based on the pure elastic and elastoplastic solutions as well.

2. GRAPHICAL APPROACH FOR WELLBORE DRILLING BOUNDARY VALUE PROBLEM

2.1. Deviatoric stress path for wellbore drilling problem

A cylindrical cavity, denoting the wellbore, is subjected to a monotonically decreasing mud pressure p_w at the wellbore surface under the initial hydrostatic stress field σ_0, as schematically shown in Fig. 1. In the rest of this paper, the mud pressure p_w may also be replaced by the radial stress at the wellbore surface σ_a. The initial radius of the wellbore, a_0, gradually decreases to the current one a. The current radius of the elastic-plastic interface is represented by r_{ep}. The pore pressure is equal to the wellbore support pressure during the drained drilling process. Note that the wellbore support pressure can go beyond the wellbore collapse pressure. Furthermore, the compressive stress is positive, which is consistent with the sign convention in geotechnical and petroleum engineering.

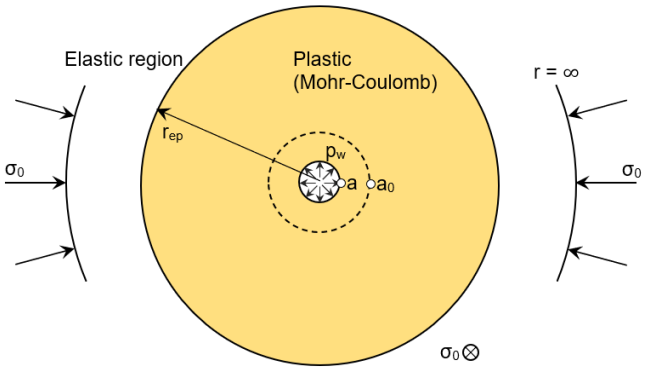

Fig. 1. Wellbore boundary value problem.

As illustrated in Chen and Abousleiman (2023), the essential feature of the graphical method for solving the cavity problem is to track the stress path through decomposing the stress and strain states/increments of a material point in the deviatoric plane. A rock element at the wellbore surface **X** (Fig. 2) is thus chosen as the representative in the graphical analysis-based for the cavity contraction problem. Its current deviatoric stress

state is denoted by point $\mathbf{X}(s_r, s_\theta, s_z)$, where s_r, s_θ, and s_z are the radial, tangential, and vertical deviatoric stress components, respectively. Likewise, the initial deviatoric stress state $\mathbf{X_0}(s_{r0}, s_{\theta 0}, s_{z0})$ indeed overlaps with the origin O, while the deviatoric stress state corresponding to the elastic-plastic transition stress state is marked by point $\mathbf{X_{ep}}(s_{r,ep}, s_{\theta,ep}, s_{z,ep})$ in Fig. 2. The final stress state is represented by $\mathbf{X_f}(s_{rf}, s_{\theta f}, s_{zf})$, which indicates that the final radial stress σ_{af}, namely the final wellbore pressure p_{wf}, vanishes at the wellbore surface. The mean stress p, the deviatoric stress q, and the deviatoric stress components can be given as follows:

$$p = \frac{1}{3}(\sigma_r + \sigma_\theta + \sigma_z) \tag{1a}$$

$$q = \sqrt{\frac{1}{2}[(\sigma_r - \sigma_\theta)^2 + (\sigma_r - \sigma_z)^2 + (\sigma_\theta - \sigma_z)^2]} \tag{1b}$$

$$s_r = \sigma_r - p = \frac{2}{3}q\sin(\theta + \frac{2\pi}{3}) \tag{1c}$$

$$s_\theta = \sigma_\theta - p = \frac{2}{3}q\sin\theta \tag{1d}$$

$$s_z = \sigma_z - p = \frac{2}{3}q\sin(\theta - \frac{2\pi}{3}) \tag{1e}$$

in which θ is the Lode angle, and its value increases clockwise from the grey line with $\theta = 0$, as depicted in Fig. 2. σ_r, σ_θ, and σ_z denote, respectively, the principal stress along the radial, tangential, and vertical directions.

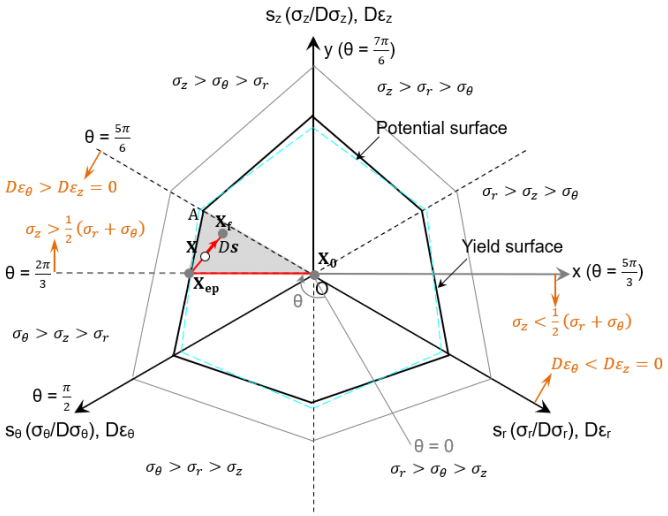

Fig. 2. Graphical representation of stress state/path in deviatoric plane for a rock element during wellbore drilling process under hydrostatic in-situ stress field with $\sigma_\theta > \sigma_z > \sigma_r$.

The projection of the pure elastic stress path on the deviatoric plane is a horizontal line from points $\mathbf{X_0}$ to $\mathbf{X_{ep}}$, as represented by segment $\mathbf{X_0X_{ep}}$ in the sector of $\frac{\pi}{2} < \theta < \frac{5\pi}{6}$ in Fig. 2 (Chen, 2024). The elastic-plastic stress state at point $\mathbf{X_{ep}}$ should satisfy the following yield function $F_{\theta r}(\sigma_\theta, \sigma_r)$ with respect to σ_r and σ_θ,

$$F_{\theta r}(\sigma_\theta, \sigma_r) = \frac{\sigma_\theta - \sigma_r}{2} - \frac{\sigma_\theta + \sigma_r}{2}\sin\phi - c\cos\phi = 0 \tag{2}$$

where ϕ is the friction angle and c is the cohesion.

According to Eq. (2), $\sigma_{r,ep}$, $\sigma_{\theta,ep}$, and $\sigma_{z,ep}$, denoting the radial, tangential, and vertical stresses at point $\mathbf{X_{ep}}$, can be obtained as:

$$\sigma_{r,ep} = (1 - \sin\phi)\sigma_0 - c\cos\phi \tag{3a}$$

$$\sigma_{\theta,ep} = (1 + \sin\phi)\sigma_0 + c\cos\phi \tag{3b}$$

$$\sigma_{z,ep} = \sigma_0 \tag{3c}$$

On the other hand, a relationship between the radial and tangential stress increments at $\mathbf{X_{ep}}$, say $D\sigma_{r,ep}$ and $D\sigma_{\theta,ep}$, can be obtained from Eq. (2) through applying the consistency condition, which is:

$$D\sigma_{\theta,ep} = \alpha D\sigma_{r,ep} \tag{4}$$

where $\alpha = \frac{1+\sin\phi}{1-\sin\phi}$.

The potential surface/function $P_{\theta r}(\sigma_\theta, \sigma_r)$ corresponding to the first yielding is illustrated in Fig. 2 by a cyan dashed hexagon passing through point $\mathbf{X_{ep}}$, which is also independent on σ_z and given by:

$$P_{\theta r}(\sigma_\theta, \sigma_r) = \frac{\sigma_\theta - \sigma_r}{2} - \frac{\sigma_\theta + \sigma_r}{2}\sin\psi - c^*_{\theta r}\cos\psi \tag{5}$$

where ψ is the dilation angle and $c^*_{\theta r}$ is a constant parameter related to the point $\mathbf{X_{ep}}$.

It is readily known that the plastic vertical/axial strain increment $D\varepsilon_z^p$ does not exist with the aid of Eq. (5), say $D\varepsilon_z^p = \lambda_{\theta r}\frac{\partial P_{\theta r}}{\partial \sigma_z} = 0$, where $\lambda_{\theta r}$ is a plastic multiplier (Chen, 2024). Note that the total strain increment along the vertical/axial direction should also be zero, i.e., $D\varepsilon_z = 0$. The combination of $D\varepsilon_z^p = D\varepsilon_z = 0$ and the generalized Hooke's law results in a relationship about three principal stress increments, namely $D\sigma_{z,ep} = \nu(D\sigma_{r,ep} + D\sigma_{\theta,ep})$, with ν representing the Poisson's ratio (Yu & Houlsby, 1991; Chen, 2024). The incremental stress ratio at point $\mathbf{X_{ep}}$ is thus given by:

$$\begin{aligned} D\sigma_{r,ep} : D\sigma_{\theta,ep} : D\sigma_{z,ep} &= 1 : \alpha : \nu(1+\alpha) \\ &= (1 - \sin\phi) : (1 + \sin\phi) : 2\nu \end{aligned} \tag{6}$$

Eq. (6) shows that the ratio of the incremental stress is merely determined by the Poisson's ratio ν and the friction angle ϕ. Therefore, the subsequential deviatoric stress path after point $\mathbf{X_{ep}}$ is a straight line, i.e., segment $\mathbf{X_{ep}X_f}$, provided the principal stresses satisfy $\sigma_\theta > \sigma_z > \sigma_r$ (Chen, 2024). Note that the colon in Eq. (6) is adopted to denote the ratio of incremental stresses, which may cause confusion with the double dot-product for tensors.

The orientation of the deviatoric stress path in the sextant of $\sigma_\theta > \sigma_z > \sigma_r$ can be described by the incremental Lode angle of $D\boldsymbol{s}$ at point $\mathbf{X}$, $\theta_{D\boldsymbol{s}}$, and analytically solved with the aid of Eq. (6), which is:

$$\theta_{Ds} = \pi + \tan^{-1}\left(\frac{1}{\sqrt{3}}\frac{1+3\sin\phi-2\nu}{1-2\nu-\sin\phi}\right) \quad (7)$$

Indeed, the direction of the elastoplastic deviatoric stress path can also be graphically illustrated following a similar procedure proposed by Chen (2024). Recalling the drilling condition ($D\sigma_r < 0$) and Eq. (6) lead to

$$D\sigma_z = \nu(1+\alpha)D\sigma_r \geq \frac{1}{2}(1+\alpha)D\sigma_r$$
$$= \frac{1}{2}(D\sigma_r + D\sigma_\theta) \quad (8a)$$

$$Dp = \frac{1}{3}(D\sigma_r + D\sigma_\theta + D\sigma_z)$$
$$= \frac{1}{3}(1+\nu)(1+\alpha)D\sigma_r \leq 0 \quad (8b)$$

with Dp denoting the increment of mean stress at point **X**. Eqs. (8a) and (8b) reveal that the deviatoric stress path $\mathbf{X_{ep}X}$ should move upwards and inwards to the negative s_r-axis of $\theta = \frac{5\pi}{6}$. Furthermore, the orientation of the elastoplastic stress path $\mathbf{X_{ep}X}$ in the drained cavity contraction problem presents an opposite trend compared to the one in the drained cavity expansion case in Mohr-Coulomb rock mass (Chen, 2024). The mathematical expression of the orientation of $\mathbf{X_{ep}X}$ can be found in Wang et al. (2024).

It is predictable that the deviatoric stress path will move towards and reach a certain point $\mathbf{X_{pr}}(s_{r,pr}, s_{\theta,pr}, s_{z,pr})$ ($\mathbf{X_{pr}}$ is not given in Fig. 2) on the negative s_r-axis as long as the wellbore pressure does not decrease to zero in the main sector of $\frac{\pi}{2} < \theta < \frac{5\pi}{6}$. According to the graphical analysis, the deviatoric stress path will stick to the negative s_r- axis after passing through point $\mathbf{X_{pr}}$. However, the corresponding proof will be omitted here since the stress path and stress state after point $\mathbf{X_{pr}}$ are not the main objectives in this work but are discussed at length by Wang et al. (2024).

2.2. Elastoplastic solution for wellbore drilling problem

The next step is to calculate the variation of the wellbore support pressure with the contracted wellbore radius after determining the orientation of the stress path in the deviatoric plane.

The constitutive equation for the point **X** as long as σ_z is strictly the intermediate principal stress in the sector of $\frac{\pi}{2} < \theta < \frac{5\pi}{6}$ can be given by (Chen & Wang, 2022):

$$\begin{bmatrix} D\sigma_r \\ D\sigma_\theta \\ D\sigma_z \end{bmatrix} = \frac{1}{\Delta}\begin{bmatrix} b_{22} & b_{21} & b_{23} \\ b_{12} & b_{11} & b_{13} \\ b_{32} & b_{31} & b_{33} \end{bmatrix}\begin{bmatrix} D\varepsilon_r \\ D\varepsilon_\theta \\ D\varepsilon_z \end{bmatrix} \quad (9)$$

where Δ and b_{ij} ($i,j = 1, 2, 3$) are all constants depending on ν, ϕ, ψ, and the shear modulus G, which have the same definitions as those in Chen and Wang (2022). $D\varepsilon_r$, $D\varepsilon_\theta$, $D\varepsilon_z$ are radial, tangential, and vertical incremental strains, respectively.

From Eq. (9) and introducing that $D\varepsilon_z = 0$:

$$D\sigma_r = \frac{1}{\Delta}[b_{22}D\varepsilon_v + (b_{21} - b_{22})D\varepsilon_\theta] \quad (10)$$

where $D\varepsilon_v = D\varepsilon_r + D\varepsilon_\theta$ denotes the volumetric strain increment.

On the other hand, the radial equilibrium equation for the borehole drilling problem can be expressed as:

$$\frac{\partial\sigma_r}{\partial r} + \frac{\sigma_r - \sigma_\theta}{r} = 0 \quad (11)$$

Note that Eq. (11) is given in the Eulerian description and can be converted into the Lagrangian form for tracking a rock element at the wellbore wall by introducing such an auxiliary variable that $\xi = \frac{a-a_0}{a}$ (Chen, 2012; Chen & Abousleiman, 2013; 2023). The combination of Eqs. (10) and (11) leads to variations of the volumetric strain and radial cavity pressure increments for point **X**, $D\varepsilon_{v,a}$ and $D\sigma_a$, which are, respectively:

$$\frac{D\varepsilon_{v,a}}{D\xi} = -\frac{\Delta}{b_{22}}\left\{-\frac{D\sigma_a}{D\xi} + \frac{b_{22}-b_{21}}{\Delta(1-\xi)}\right\} \quad (12)$$

$$\frac{D\sigma_a}{D\xi} = -\frac{\sigma_a - \sigma_{\theta,a}}{1-\xi-\frac{e^{\varepsilon_{v,a}}}{1-\xi}} \quad (13)$$

where $\sigma_{\theta,a}$ is the tangential stress increments pertaining to a rock element in the wellbore surface.

A first-order differential equation of σ_a can, therefore, be derived from Eq. (13) with Eq. (12), giving:

$$\frac{D\sigma_a}{D\xi} = -\frac{(1-\alpha)\sigma_a - Y}{1-\xi-\frac{1}{1-\xi}\exp\left[\frac{\Delta}{b_{22}}\sigma_a + \frac{b_{22}-b_{21}}{b_{22}}\ln(1-\xi)+C\right]} \quad (14)$$

where the constant coefficients in the above equation can be given by:

$$Y = \frac{2c\cos\phi}{1-\sin\phi} \quad (15a)$$

$$C = -\frac{\Delta}{b_{22}}\sigma_{a,ep} - \frac{b_{22}-b_{21}}{b_{22}}\ln(1-\xi_{ep}) \quad (15b)$$

$$\xi_{ep} = \frac{\sigma_{a,ep}-\sigma_0}{2G} \quad (15c)$$

$\sigma_{a,ep}$ is the wellbore pressure at the elastoplastic transition point $\mathbf{X_{ep}}$ pertaining to the initial yielding wellbore pressure, which can be readily determined from Eq. (3a). Thus, the wellbore pressure for point **X** in the sector of $\frac{\pi}{2} < \theta < \frac{5\pi}{6}$ can be straightforwardly evaluated by numerically integrating Eq. (14) from the starting point $\mathbf{X_{ep}}$.

3. NUMERICAL RESULTS

Some values of rock parameters are chosen in this section to investigate their influence on the normalized wellbore

drilling curve ($\frac{p_w}{\sigma_0}$ versus $\frac{a_0}{a}$) if the vertical/axial stress is strictly intermediate principal stress during the drilling process. The prediction of the critical mud pressure $p_{w,cr}$ for maintaining the wellbore stability can be drawn from the wellbore pressure-drilling (contraction) curves. The following normalized values of rock parameters are used in the examples calculations: shear modulus $\frac{G}{\sigma_0} = 100$, 200, and 300; Poisson's ratio $\nu = 0.25$; cohesion $\frac{c}{\sigma_0} =$ 0.2, 0.3, and 0.4; friction angle $\phi = 35°$, 40°, and 45°, the dilation angle $\psi = 10°$, with $\frac{G}{\sigma_0} = 100$ $\nu = 0.25$, $\frac{c}{\sigma_0} = 0.2$, $\phi = 35°$, and $\psi = 10°$ being the reference case.

Fig. 3 presents the variation of the normalized wellbore support pressure $\frac{p_w}{\sigma_0}$ for three different values of the friction angle $\phi = 35°$, 40°, and 45°. The values of normalized shear modulus and cohesion are chosen as $\frac{G}{\sigma_0} = 100$ and $\frac{c}{\sigma_0} = 0.2$, respectively. As curves shown in Fig. 3, a stiffer normalized wellbore drilling curve happens to the one with a larger friction angle ϕ. In other words, a larger value of the friction angle ϕ leads to a smaller contraction of the wellbore surface at the same level of the decreased wellbore support pressure p_w.

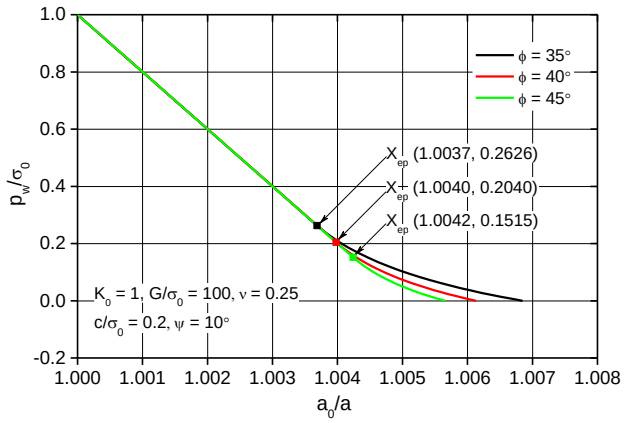

Fig. 3. Variation of normalized wellbore support pressure with normalized wellbore radius for different values of the friction angle.

Figs. 4 and 5 show influences of the normalized cohesion and shear modulus on the wellbore drilling curves, respectively. In Fig. 4, the values of the normalized cohesion $\frac{c}{\sigma_0}$ are taken as 0.2, 0.3, and 0.4 with the shear modulus $\frac{G}{\sigma_0} = 100$ and friction angle $\phi = 35°$. While the value of $\frac{c}{\sigma_0}$ is 0.2 and the values of $\frac{G}{\sigma_0}$ are 100, 200, and 300 for curves in Fig. 5. It can be seen that a larger value of $\frac{c}{\sigma_0}$ or $\frac{G}{\sigma_0}$ also results in a smaller radial contraction displacement at the wellbore wall.

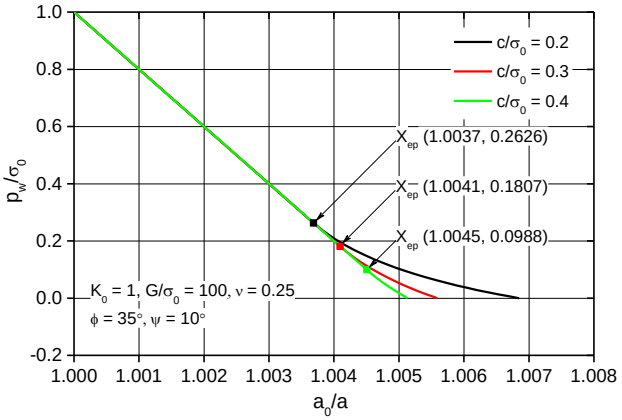

Fig. 4. Variation of normalized wellbore support pressure with normalized wellbore radius for different values of normalized cohesion.

The critical mud pressure $p_{w,cr}$ is the threshold value of the wellbore support pressure to prevent the borehole collapse during the drilling process for the wellbore design. The critical mud pressure $p_{w,cr}$ can be determined based on the elastic and elastoplastic analyses for rock formation obeying the perfect Mohr-Coulomb model (Chen, 2012). Based on the elastic criterion, the critical mud pressure $p_{w,cr}^e$ is usually defined as corresponding to the wellbore pressure for which the borehole surface is just entering the yielding/failure state (Mohr-Coulomb failure criterion herein). While the critical wellbore pressure, $p_{w,cr}^p$, pertaining to the elastoplastic criterion can be determined based on the allowable inward displacement at the borehole surface, e.g., a tolerance borehole surface strain of $\varepsilon = \frac{a_0 - a}{a}$ set in between 2% and 5% (Charlez, 1997; Charlez & Heugas, 1991).

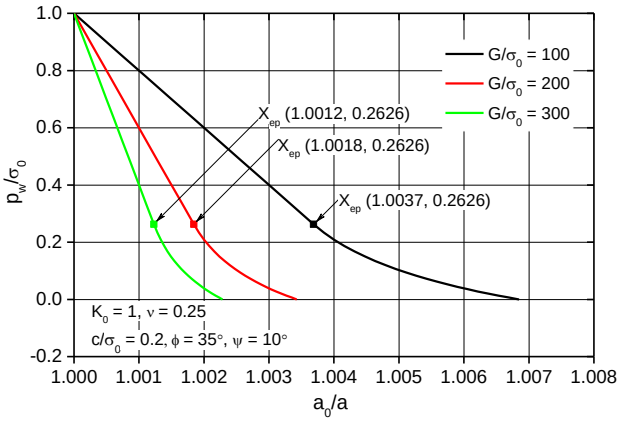

Fig. 5. Variation of normalized wellbore support pressure with normalized wellbore radius for different values of normalized shear modulus.

The normalized critical mud pressure pertaining to the elastic and elastoplastic analyses, $\frac{p_{w,cr}^e}{\sigma_0}$ and $\frac{p_{w,cr}^p}{\sigma_0}$, can be directly obtained from the normalized wellbore drilling curves. For instance, from Fig. 3, the elastic critical

wellbore pressure $\frac{p^e_{w,cr}}{\sigma_0}$ are 0.2626, 0.2040, and 0.1515, with the corresponding borehole surface strain $\varepsilon =$ 0.37%, 0.40%, and 0.42% for the case of $\phi = 35°$, 40°, and 45°, respectively, as presented by points $\mathbf{X_{ep}}$ therein. Likewise, $\frac{p^e_{w,cr}}{\sigma_0}$ and ε related to points $\mathbf{X_{ep}}$ for considerations of influences of the normalized cohesion $\frac{c}{\sigma_0}$ and $\frac{G}{\sigma_0}$ are shown in Figs. 4 and 5 as well, respectively. It is evidently noticed that, however, the corresponding elastoplastic strain ε for all the cases of the given values of rock parameters in these numerical examples are smaller than 2%, even if the wellbore support pressure has decreased to zero. This phenomenon indicates that the wellbore under such combinations of rock parameters can be considered as self-stabilization without mud support during the drilling process.

4. CONCLUSIONS

This paper focuses on the development of a rigorous analytical solution for the drained wellbore drilling problem in a non-associated Mohr-Coulomb rock under hydrostatic in-situ stress field, for a specific case that the axial/vertical stress remains strictly intermediate during the drilling process. The analytical solution for the wellbore support pressure for such a specific scenario is derived following the graphical method developed by Chen (2024) for the case of the drained cavity expansion problem under arbitrary in-situ stress fields, which can be numerically calculated through a first-order differential equation. The graphical method, as a novel and rigorous analytical approach, avoids the unnecessary assumption of the intermediacy of the axial/vertical stress (Chen & Wang, 2022; Chen, 2024). It is found that the deviatoric stress path of a representative rock element in the wellbore wall consists of two piecewise straight lines that correspond to the purely elastic and elastoplastic deformation stages, respectively. The wellbore support pressure is numerically calculated with the aid of the radial equilibrium equation in the Lagrangian form, for stress state located in the sextant of $\frac{\pi}{2} < \theta < \frac{5\pi}{6}$.

Influences of rock parameters, friction angle, cohesion, and shear modulus, on the wellbore support pressure and inward radial displacement are illustrated through normalized wellbore drilling curves. Results show that a higher value of the friction angle, the cohesion, or the shear modulus lead to smaller wellbore wall radial displacement, which implies lower critical mud pressure for maintaining wellbore stability during drilling. It is also found that, with the specific rock parameters taken in the present numerical analyses, the wellbore can well remain stable even under the fully unsupported drilling condition.

ACKNOWLEDGEMENT

The work reported in this paper is partially funded by the Industrial Ties Research Subprogram of the Louisiana Board of Regents [Grant No. LEQSF(2019-22)-RD-B-01].

NOTATION

a	current wellbore radius
a_0	initial wellbore radius
b_{ij}	constant elements of elastoplastic constitutive matrix $(i,j = 1,2,3)$
C, Y	constant parameters related to wellbore support pressure
c	cohesion
$c^*_{\theta r}$	constant parameter in $P_{\theta r}$
$D\boldsymbol{s}$	deviatoric stress increment vector
$D\varepsilon_r, D\varepsilon_\theta, D\varepsilon_z$	total strain increments of a given material particle in radial, tangential, and vertical directions
$D\varepsilon_v$	volumetric strain increment
$D\varepsilon_{v,a}$	volumetric strain increment at the wellbore wall
$D\varepsilon^p_z$	plastic vertical strain increment at stress state **X**
$D\sigma_{r,ep}, D\sigma_{\theta,ep}, D\sigma_{z,ep}$	radial, tangential, and vertical stress increments at transition state $\mathbf{X_{ep}}$
$F_{\theta r}$	Mohr-Coulomb yield function
G	Shear modulus
p	mean stress invariant
p_w	mud pressure
$p_{w,cr}$	critical mud pressure
$p^e_{w,cr}$	critical mud pressure determined from elastic solution
$p^p_{w,cr}$	critical mud pressure determined from elastic-plastic solution
p_{wf}	final wellbore pressure
$P_{\theta r}$	potential function for stress state **X**
q	deviatoric stress invariant
r	radius of arbitrary rock element around wellbore
r_{ep}	current elastic-plastic interface
s_r, s_θ, s_z	stress deviator components in radial, tangential, and vertical principal directions
$s_{r0}, s_{\theta 0}, s_{z0}$	stress deviator components in radial, tangential, and vertical principal directions of the initial stress state
$s_{r,ep}, s_{\theta,ep}, s_{z,ep}$	stress deviator components in radial, tangential, and vertical principal directions of the elastic-plastic transition
$s_{rf}, s_{\theta f}, s_{zf}$	stress deviator components in radial, tangential, and vertical principal directions at the final stress state

$s_{r,pr}, s_{\theta,pr}, s_{z,pr}$	stress deviator components in radial, tangential, and vertical principal directions at point $\mathbf{X_{pr}}$
$\mathbf{X}$	current stress state projected on sextant $\frac{\pi}{2} < \theta < \frac{5\pi}{6}$ of the π-plane
$\mathbf{X_0}$	in situ stress state projected on the π-plane
$\mathbf{X_{ep}}$	elastic-plastic transition stress state in the deviatoric plane
$\mathbf{X_f}$	final stress state in the deviatoric plane
$\mathbf{X_{pr}}$	intersection point of plastic stress path with the negative s_r axis in deviatoric plane
α	constant parameter of Mohr-Coulomb properties
Δ	constant parameter involved in the elastoplastic stiffness matrix
ε	tolerance borehole surface strain
θ	Lode angle
$\theta_{D\boldsymbol{s}}$	Lode angle of $D\boldsymbol{s}$
$\lambda_{\theta r}$	plastic multiplier
ν	Poisson's ratio
ξ	auxiliary variable
ξ_{ep}	auxiliary variable at stress state $\mathbf{X}$
σ_0	hydrostatic in situ total stress
σ_a	wellbore support pressure
σ_{af}	final radial stress
$\sigma_r, \sigma_\theta, \sigma_z$	stress components in radial, tangential, and vertical directions
ϕ	friction angle
ψ	dilation angle

REFERENCES

1. Al-Ajmi, A. M. & Zimmerman, R. W. (2006). Stability analysis of vertical boreholes using the Mogi–Coulomb failure criterion. *Int. J. Rock Mech. Min. Sci*., 43(8):1200–1211.
2. Bradley, W. B. (1979). Failure of inclined boreholes. *J. Energy Resour. Tech*., 101:232-239.
3. Carter, J. P. and Booker, J. R. (1982). Elastic consolidation around a deep circular tunnel. *Int. J. Solids Struct.*, 18(12):1059-1074.
4. Chadwick, P. (1959). The quasi-static expansion of a spherical cavity in metals and ideal soils. *Q. J. Mech. Appl. Math.*, 12(1):52-71.
5. Charlez, P. A. (1997). *Rock mechanics. Volume 2: petroleum application*. Editions Technip, Paris.
6. Charlez, P. A. & Heugas, O. (1991). Evaluation of optimal mud weight in soft shale levels. *Rock Mechanics as a multidisciplinary science* (Editor: Roegiers, J. C.), pages 1005-1014. Balkema, Rotterdam.
7. Chen, S. L. (2012). *Analytical and numerical analyses of wellbore drilled in poroelastoplastic rock formations* (Publication No. 3549292) [Doctoral dissertation, University of Oklahoma]. ProQuest Dissertations Publishing.
8. Chen, S. L. (2024). A graphical solution framework for elastoplastic cylindrical cavity problem in Mohr-Coulomb material. *J. Eng. Mech*. 150(5): 04024016.
9. Chen, S. L. & Abousleiman, Y. N. (2013). Exact drained solution for cylindrical cavity expansion in modified Cam Clay soil. *Géotechnique*, 63(6):510-517.
10. Chen, S. L. & Abousleiman, Y. N. (2023). A graphical analysis-based method for undrained cylindrical cavity expansion in modified cam clay soil. *Géotechnique*, 73(8): 736-746.
11. Chen, S. L., Abousleiman, Y. N., and Muraleetharan, K. K. (2012). Closed-form elastoplastic solution for the wellbore problem in strain hardening/softening rock formations. *Int. J. Geomech.*, 12(4):494-507.
12. Chen, S. L. & Wang, X. (2022). A graphical method for undrained analysis of cavity expansion in Mohr-Coulomb soil. *Géotechnique*, https://doi.org/10.1680/jgeot.22.00088.
13. Cui, L., Cheng, A. H-D. & Abousleiman, Y. (1997). Poroelastic solution for an inclined borehole. *J. Appl. Mech*., 64:32-38.
14. Detournay, E. and Cheng, A. D. (1988). Poroelastic response of a borehole in a non-hydrostatic stress field. *Int. J. Rock Mech. Sci. & Min. Sci. & Geomech*., Abstr. 25(3):171-182.
15. Florence, A. L. & Schwer, L. E. (1978). Axisymmetric compression of a Mohr–Coulomb medium around a circular hole. *Int. J. Numer. Anal. Mech. Geomech*., 2(4):367-379.
16. Huang, C., Akbari, B., and Chen, S. (2018). Quick approximate elastoplastic solutions of wellbore stability problems based on numerical simulation and statistical analysis. J. Nat. Gas Sci. Eng., 51:147-154.
17. Ito, T., Kurosawa, K., and Hayashi, K. (1998). Stress concentration at the bottom of a borehole and its effect on borehole breakout formation. Rock Mech. Rock Eng., 31:153-168.
18. Kanfar, M. F., Chen, Z & Rahman, S. S. (2015). Effect of material anisotropy on time-dependent wellbore stability. *Int. J. Rock Mech. Min. Sci*., 78:36–45.
19. Mehrabian, A. & Abousleiman, Y. N. (2013). Generalized poroelastic wellbore problem. *Int J. Numer. Anal. Met*., 37:2727–2754.
20. Papanastasiou, P. & Zervos, A. (2004). Wellbore stability analysis: from linear elasticity to postbifurcation modeling. *Int. J. Geomech., ASCE*, 4(1):2-12.
21. Potts, D. M. & Zdravkovic, L. (1999). Finite element analysis in geotechnical engineering: theory. Thomas Telford Ltd.
22. Reed, M. B. (1988). The influence of out-of-plane stress on a plane strain problem in rock mechanics. *Int. J. Numer. Anal. Mech. Geomech*., 12:173-181.
23. Risnes, R., Bratli, R. K. & Horsrud, P. (1982). Sand stresses around a wellbore. *SPE J*., 22(6):883-898.
24. Vesic, A. C. (1972). Expansion of cavities in infinite soil mass. *J. Soil Mech. Found. Div*. ASCE 98(SM3):265-290.
25. Wang, X., Chen, S. L., Han, Y. H. & Abousleiman, Y. N. (2024). An analytical drained solution based on graphical method for wellbore drilling problem in dilatant Mohr-Coulomb rock formations. Submitted to *Int. J. Rock Mech. Min. Sci.*

26. Yu, H. S. & Houlsby, G. T. (1991). Finite cavity expansion in dilatant soils: loading analysis. *Géotechnique*, 41(2):173-183.
27. Zoback, M. D., Barton, C. A., Brudy, M., Castillo, D. A., Finkbeiner, T., Grollimund, B. R., Moos, D. B., Peska, P., Ward, C. D., and Wiprut, D. J. (2003). Determination of stress orientation and magnitude in deep wells. *Int. J. Rock Mech. Min. Sci*., 40(7-8):1049-1076.